LETTER Communicated by Douglas Fields

Oscillations and Spiking Pairs: Behavior of a Neuronal Model with STDP Learning

Xi Shen
victorshenshx@gmail.com
Department of Electrical and Electronic Engineering, Imperial College London, London SW7 2BT, U.K.

Xiaobin Lin
XL61@hw.ac.uk
Philippe De Wilde
pdw@macs.hw.ac.uk
Department of Computer Science, Heriot-Watt University, Edinburgh EH14 4AS, U.K.

In a biologically plausible but computationally simplified integrate-and-fire neuronal population, it is observed that transient synchronized spikes can occur repeatedly. However, groups with different properties exhibit different periods and different patterns of synchrony. We include learning mechanisms in these models. The effects of spike-timing-dependent plasticity have been known to play a distinct role in information processing in the central nervous system for several years. In this letter, neuronal models with dynamical synapses are constructed, and we analyze the effect of STDP on collective network behavior, such as oscillatory activity, weight distribution, and spike timing precision. We comment on how information is encoded by the neuronal signaling, when synchrony groups may appear, and what could contribute to the uncertainty in decision making.

1 Introduction

To unravel the mystery of information processing in the brain, neurophysiologists are measuring the firing patterns of neurons both in vivo and in vitro. Some experiments revealed synchronized discharges in a population of neurons (see, e.g., Kreiter & Singer, 1996), indicating that the spikes are collectively organized to some extent. Other researchers discovered precisely reproducible spike time patterns (see, e.g., Mainen & Sejnowski, 1995; Reinagel & Reid, 2000), suggesting that information may be coded in spike time as well. In addition, the synapses in the brain are obviously not static. The first description of associative synaptic modification, long-term potentiation (LTP), was given in the 1970s (Bliss & Gardner-Medwin, 1973; Bliss & Lømo, 1973). Various experiments since then have indicated

that the temporal order of the pre- and postsynaptic activation was crucial to activity-induced synaptic modification. Long-term depression (LTD) exists as the reversed effect of LTP (Kelso & Brown, 1986). As an exclusive summing up of LTP, LTD, and other related behavior, the notion of spike-timing-dependent plasticity (STDP) was introduced in 2000 (Song, Miller, & Abbott, 2000). Since then, the STDP modification function has drawn much attention because it reflects the fundamental principles for mental tasks such as learning and memory in the brain. Because of the enormous complexity and variability of brain activity, numerous phenomena have been observed but not explained. More and more findings, however, are making us believe that the task of understanding the brain is not insurmountable.

Oscillations have been observed in both experimental and analytical studies on neural networks. The phenomenon of collective synchronization is commonly observed in biology and physics; the firing time difference among a subgroup of synchronized neurons is found with a precision of ± 4 microseconds (Beggs & Plenz, 2004; Segev, Baruchi, Hulata, & Ben-Jacob, 2004). Synchronization has been well studied using coupled oscillator models at the same time (see, e.g., Strogatz, 2000; Strogatz, Mirollo, & Matthews, 1992). The notion of oscillation is sightly different in neuroscience, it is simply defined to refer to the tendency of the neuronal population, under certain parameter conditions, to oscillate between a state where no neurons are firing to a state where a large percentage of the neurons are firing simultaneously. Although it is still uncertain how information is coded in oscillations, multiple experimental discoveries and simulation results suggest that oscillatory behavior plays an important role in many functions carried out by the brain.

Which model to use is an important issue for our investigation. There are various integrate-and-fire neuronal models to choose from. To capture the gist of the these models, an overview with comparisons between models is required, and a detailed analysis of all variables and parameters is also important. These analyses will lead to a biologically plausible but computationally simplified integrate-and-fire neuronal model with balanced excitatory and inhibitory neurons. This model will be suitable for large-scale simulations so that the emergent behavior can easily be observed.

In our study, we also take STDP into account. On the one hand, the STDP performs as internal perturbations in neuronal populations because it acts on the connections between neurons. On the other hand, it is a learning mechanism as it is activity dependent and modulates the signaling between neurons. The behavior of neuronal populations coupled with STDP algorithms is explored in this letter.

2 Basic Description of IF Models

Integrate-and-fire (IF) neuronal models are very popular for theoretical studies on populations of neurons, especially for large-scale simulations.

We start reviewing different versions of IF models used in recent papers. IF models have three major components: the postsynaptic potential or current, the membrane potential, and the firing threshold. Normally, they are described by differential equations.

2.1 Postsynaptic Current/Potential. In Amit and Brunel's model (1997), the postsynaptic current is denoted by

$$\tau' \dot{I}(t) = -I(t) + \sum_{i=1}^{C} w_i \tau \sum_k \delta\left(t_i^k - t\right), \tag{2.1}$$

where τ' and τ are two constants that control the decay rate. It is easy to see that $\sum_{i=1}^{C} w_i \tau \sum_k \delta(t_i^k - t)$ is just a series of weighted delta functions, representing all afferent presynaptic spikes.

Panchev and Wermter (2004) use the following equation to describe the postsynaptic current:

$$\tau \frac{d}{dt} I(t) = -I(t) + \sum_{j \in \varphi} w_j \sum_{t^k \in \hbar^j} \rho(\Delta t^k) \delta(t - t^k), \tag{2.2}$$

in which the function ρ is for the dynamics of synapses. If we ignore it, this equation is the same as equation 2.1.

Another formula, proposed by Melamed, Silberberg, Markram, Gerstner, and Richardson (2005) is as follows:

$$I(t) = \frac{q}{\tau} \sum_{t^k} \Theta(t - t^k) \exp\left(- \frac{t - t^k}{\tau} \right), \tag{2.3}$$

where $\Theta(t)$ is the Heaviside step function. Note that this equation is not a differential equation; it is already a solution. Here the postsynaptic current is just the sum of all the afferent exponentially decaying spikes (see the middle panel in Figure 1).

Brunel and Hakim (1999) mentioned the following equation as the α-function with a latency τ_L:

$$RI_i(t) = \tau \sum_j w_{ij} \sum_k f\left(t - t_j^k\right), \tag{2.4}$$

in which

$$f(t) = \begin{cases} \dfrac{t - \tau_L}{\tau_s^2} \exp\left(- \dfrac{t - \tau_L}{\tau_s} \right) & \text{for } t > \tau_L \\ 0 & \text{otherwise.} \end{cases}$$

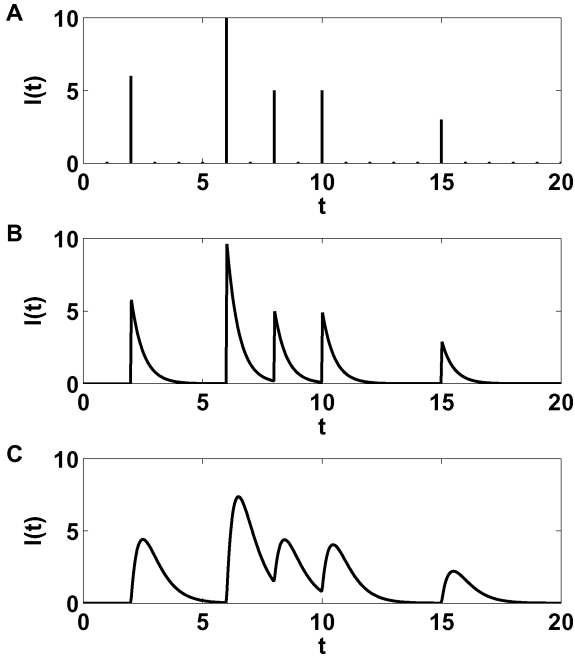

Figure 1: Different behavior of the postsynaptic current described by equations; transmission delays are not taken into account. (A) Plot of equation 2.5 when the afferent current is a series of spikes. (B) The jump-and-decay behavior of the current in equation 2.3 with the same incoming spikes, in which $\tau = 0.5$. (C) The locus of the postsynaptic current dominated by equation 2.4 with the same incoming spikes, $\tau_s = 0.5$.

And in Giudice, Fusi, and Mattia's model (2003), the postsynaptic current is defined by a very simple equation:

$$I(t) = \sum_j w_j \sum_k \delta\left(t - t_j^k - d_j^k\right), \tag{2.5}$$

where j labels the afferent synapses, k denotes different spikes from one neuron, and d is the transmission delay.

Looking from equation 2.1 through to equation 2.5, it is not difficult to conclude that equation 2.5 is the simplest; it means that the postsynaptic current is just a series of weighted impulses. When there is no presynaptic spike arriving, the postsynaptic current is zero (see Figure 1A). Equation 2.3 is more realistic; the postsynaptic current "jumps" and decays after a spike arrives (see Figure 1B). The update rule in equation 2.4 is the most complicated; it looks like an approximation of the integral of equation 2.3, as shown in Figure 1C.

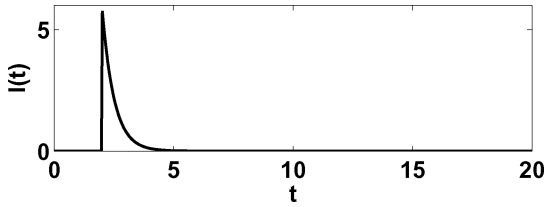

Figure 2: The solution of $I(t)$ when $w_j = 3$, $t_j^0 = 2$, $\tau_s = 0.5$, and $I(0) = 0$.

Unlike equations 2.3, 2.4, and 2.5, the postsynaptic current in equations 2.1 and 2.2 cannot be plotted directly. Here we will find an analytical solution for them first. Suppose we have the following differential equation:

$$\tau_s \frac{dI(t)}{dt} = -I(t) + w_j \delta\big(t - t_j^0\big); \tag{2.6}$$

in other words, there is only one presynaptic spike, which is from neuron j, at $t = t_j^0$. Solving equation 2.6 yields

$$\begin{aligned}
\frac{dI(t)}{dt} + \frac{I(t)}{\tau_s} &= \frac{w_j \delta\big(t - t_j^0\big)}{\tau_s}, \Longrightarrow \\
e^{\frac{t}{\tau_s}} \frac{dI(t)}{dt} + \frac{I(t)}{\tau_s} e^{\frac{t}{\tau_s}} &= \frac{1}{\tau_s} w_j \delta\big(t - t_j^0\big) e^{\frac{t}{\tau_s}}, \Longrightarrow \\
\big(I(t) e^{\frac{t}{\tau_s}}\big)' &= \frac{w_j}{\tau_s} \delta\big(t - t_j^0\big) e^{\frac{t}{\tau_s}}, \Longrightarrow \\
I(t) e^{\frac{t}{\tau_s}} &= \frac{w_j}{\tau_s} \int \delta\big(t - t_j^0\big) e^{\frac{t}{\tau_s}} dt.
\end{aligned}$$

Therefore,

$$\begin{aligned}
I(t) e^{\frac{t}{\tau_s}} &= \frac{w_j}{\tau_s} e^{\frac{t_j^0}{\tau_s}} \big(H\big(t - t_j^0\big) + C\big), \Longrightarrow \\
I(t) &= C e^{-\frac{t}{\tau_s}} + \frac{w_j}{\tau_s} H\big(t - t_j^0\big) e^{-\frac{t - t_j^0}{\tau_s}},
\end{aligned} \tag{2.7}$$

where $H(t)$ is the Heaviside step function. If $I(0) = 0$, then $C = 0$. The plot of $I(t)$ when $t_j^0 = 2$ and $\tau_s = 0.5$ can be found in Figure 2.

Even if there are multiple afferent impulses,

$$\tau_s \frac{dI(t)}{dt} = -I(t) + \sum_i^B w_i \sum_k \delta\big(t_i^k - t\big), \tag{2.8}$$

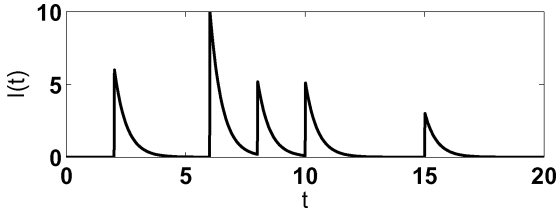

Figure 3: Plot of Borisyuk's model with the same afferent spikes as in Figure 1. The postsynaptic potential is denoted by $I(t)$ here. We can see that the curve is the same as that in the middle panel of Figure 1.

the differential equation can still be solved using the same method as above, which gives

$$I(t) = Ce^{-\frac{t}{\tau_s}} + \sum_i^B \frac{w_i}{\tau_s} \sum_k H\left(t - t_i^k\right) e^{-\frac{t-t_i^k}{\tau_s}}. \tag{2.9}$$

Indeed, it is the same as equation 2.3. Here we can conclude that equation 2.3 is just the solution of equations 2.1 and 2.2. These three equations define the same behavior. Consequently, there are three main ways of representing the postsynaptic current, and all are shown in Figure 1.

In Borisyuk's model (2002), the postsynaptic potential changes in the following manner:

$$P_{ij}(t+1) = P_{ij}(t)\exp\left(\frac{-1}{\tau_{ij}}\right) + \alpha, \tag{2.10}$$

$$\alpha = \begin{cases} w_{ij} & \text{if } t+1 = t_j^k + \Delta t_{ij} \\ 0 & \text{else,} \end{cases}$$

which is the discrete time version of the jump-and-decay behavior. We set the single step in equation 2.10 as 0.02 and simulated the model with the same afferent spikes as in Figure 1; the result is shown in Figure 3. We can see that this discrete time formula leads to satisfactory approximation.

2.2 Membrane Potential. The equations concerning the membrane potential in different integrate-and-fire models share the same form. For instance, in Amit and Brunel's (1997) model,

$$\tau_m \dot{V}(t) = -V(t) + I(t), \tag{2.11}$$

in which $I(t)$ is expressed in equation 2.1. In Panchev and Wermter's (2004) model, it is very similar:

$$\tau_m \frac{dV(t)}{dt} = -V(t) + RI(t), \tag{2.12}$$

which works together with equation 2.2. And so it is in the model used by Melamed et al. (2005),

$$\tau_m \dot{V}(t) = -V(t) + RI(t), \tag{2.13}$$

where $I(t)$ is defined in equation 2.3.

Here we use the equation in the following form:

$$\tau_m \frac{dV_m(t)}{dt} = -V_m(t) + R_m I(t). \tag{2.14}$$

We assume first that there is only one presynaptic spike and $I(0) = 0$; we will use $I(t)$ in equation 2.7, which is rewritten as

$$I(t) = \frac{w_j}{\tau_s} H\big(t - t_j^0\big) e^{-\frac{t-t_j^0}{\tau_s}}. \tag{2.15}$$

Hence,

$$\frac{dV_m(t)}{dt} = \frac{-V_m(t)}{\tau_m} + \frac{R_m w_j}{\tau_m \tau_s} H\big(t - t_j^0\big) e^{-\frac{t-t_j^0}{\tau_s}}, \tag{2.16}$$

which yields

$$\begin{aligned}
e^{\frac{t}{\tau_m}} \frac{dV_m(t)}{dt} + \frac{V_m(t)}{\tau_m} e^{\frac{t}{\tau_m}} &= A \cdot H\big(t - t_j^0\big) e^{\frac{t}{\tau_m}} e^{-\frac{t-t_j^0}{\tau_s}}, \Longrightarrow \\
\big(V_m(t) e^{\frac{t}{\tau_m}}\big)' &= A \cdot H\big(t - t_j^0\big) e^{\frac{t}{\tau_m}} e^{-\frac{t-t_j^0}{\tau_s}}, \Longrightarrow \\
V_m(t) e^{\frac{t}{\tau_m}} &= A \cdot \int H\big(t - t_j^0\big) e^{\frac{t}{\tau_m}} e^{-\frac{t-t_j^0}{\tau_s}} dt, \Longrightarrow \\
V_m(t) e^{\frac{t}{\tau_m}} &= A \cdot e^{\frac{t_j^0}{\tau_s}} \int H\big(t - t_j^0\big) e^{\alpha t} dt,
\end{aligned} \tag{2.17}$$

where

$$A = \frac{R_m w_j}{\tau_m \tau_s}, \quad \alpha = \frac{\tau_s - \tau_m}{\tau_s \tau_m}. \tag{2.18}$$

By doing the integration, we have:

$$\int H(t-t_j^0)e^{\alpha t}dt = \frac{1}{\alpha}\int H(t-t_j^0)de^{\alpha t}, \Longrightarrow$$

$$\int H(t-t_j^0)e^{\alpha t}dt = \frac{1}{\alpha}\left[H(t-t_j^0)e^{\alpha t} - \int e^{\alpha t}dH(t-t_j^0)\right], \Longrightarrow$$

$$\int H(t-t_j^0)e^{\alpha t}dt = \frac{1}{\alpha}\left[H(t-t_j^0)e^{\alpha t} - e^{\alpha t_j^0}H(t-t_j^0) + C\right].$$

With equation 2.17, it yields:

$$V_m(t)e^{\frac{t}{\tau_m}} = \frac{R_m w_j}{\tau_m \tau_s}\cdot e^{\frac{t_j^0}{\tau_s}}\cdot\frac{\tau_s\tau_m}{\tau_s-\tau_m}\left[H(t-t_j^0)e^{\alpha t} - e^{\alpha t_j^0}H(t-t_j^0)+C\right], \Longrightarrow$$

$$V_m(t) = \frac{R_m w_j}{\tau_s-\tau_m}e^{\frac{t_j^0}{\tau_s}-\frac{t}{\tau_m}}\left[H(t-t_j^0)e^{\alpha t} - e^{\alpha t_j^0}H(t-t_j^0)+C\right]. \tag{2.19}$$

Here we break it down into two parts:

$$V_1(t) = \frac{R_m w_j}{\tau_s-\tau_m}e^{\frac{t_j^0}{\tau_s}-\frac{t}{\tau_m}}\cdot C, \tag{2.20}$$

$$V_2(t) = \frac{R_m w_j}{\tau_s-\tau_m}e^{\frac{t_j^0}{\tau_s}-\frac{t}{\tau_m}}\left[H(t-t_j^0)e^{\alpha t} - e^{\alpha t_j^0}H(t-t_j^0)\right], \tag{2.21}$$

so

$$V_m(t) = V_1(t) + V_2(t).$$

The term $V_2(t)$ can be rearranged as

$$V_2(t) = \frac{R_m w_j}{\tau_s-\tau_m}\left[H(t-t_j^0)e^{(\frac{1}{\tau_m}-\frac{1}{\tau_m})t+\frac{t_j^0}{\tau_s}-\frac{t}{\tau_s}} - H(t-t_j^0)e^{(\frac{1}{\tau_m}-\frac{1}{\tau_m})t_j^0+\frac{t_j^0}{\tau_m}-\frac{t}{\tau_m}}\right];$$

therefore,

$$V_2(t) = \frac{R_m w_j}{\tau_s-\tau_m}\left[H(t-t_j^0)e^{\frac{t_j^0-t}{\tau_s}} - H(t-t_j^0)e^{\frac{t_j^0-t}{\tau_m}}\right]. \tag{2.22}$$

This equation shows that $V_2(t)$ is actually the linear combination of two decaying terms with different decay rates. This nature is very important for simulations because it can significantly reduce computational expenses, which will be explained in section 3.2.

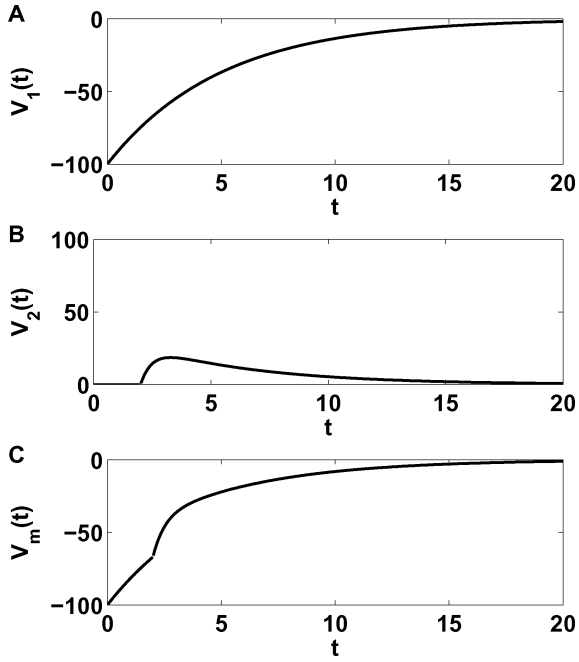

Figure 4: Plot of $V_1(t)$, $V_2(t)$, and $V_m(t)$ when the parameters are chosen as follows: $R_m = 20$, $w_j = 3$, $\tau_s = 0.5$, $\tau_m = 5$, $t_j^0 = 2$, and $C = 0.1374$ so that $V_m(0) = -100$.

If $V(0) = 0$, then $C = 0$ and $V_m(t) = V_2(t)$, the plot of $V_2(t)$ can be found in the middle panel in Figure 4. It is worth noting that $V_1(t)$ plays a dominant role in the dynamics above. When a spike arrives, $V_2(t)$ adds just a small hump to the decaying curve; nevertheless, the membrane potential always decays toward 0. However, in a real brain cell, the membrane potential is never zero; it is usually chosen in the range (−100 mV, −50 mV). In equation 2.19, C makes sure that $V_m(t)$ decays from the right value. Therefore, if we choose the reset value of the membrane potential to be realistic, $V_m(t)$ is the linear combination of a decaying part ($V_1(t)$) and a signal part ($V_2(t)$).

In Borisyuk's (2002) model, the total potential $V(t)$ is

$$V(t) = \sum_j P_j(t) + \beta_{sm} \exp\left(\frac{-(t - t^k)}{\tau_m}\right), \tag{2.23}$$

where β_{sm} is the reset value of the membrane potential after a spike is generated, and $P_j(t)$ is given by equation 2.10. In simple words, $V(t)$ here is the sum of a decaying term ($V_1(t)$ in Figure 4) and the incoming current (as in Figure 3). And this description is different from that in equation 2.19, because here the membrane potential makes jumps when there are incoming spikes.

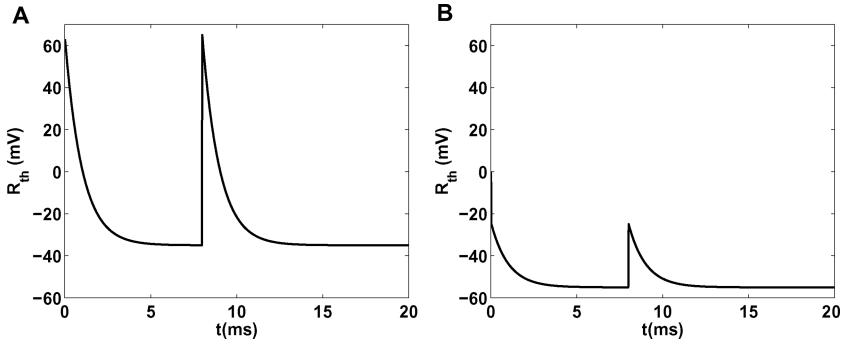

Figure 5: Plot of the threshold when there are two spikes in the time interval: $t^1 = 0$ ms and $t^2 = 8$ ms. The decay constant τ_{th} is 1 in both figures. (A) The threshold in Coombes's model. (B) The threshold in Borisyuk's model.

2.3 Threshold. In most integrate-and-fire models, the firing threshold is regarded as a constant. However, Coombes (2003) uses a more realistic decaying threshold. It is defined as

$$\tau_{th}\frac{dR_{th}}{dt} = -R_{th} + \Gamma_\infty,\ R_{th}(\sigma_n^+) = R_{th}(\sigma_n) + \Gamma_0, \tag{2.24}$$

in which Γ_∞ and Γ_0 are chosen to be -35 mV and 100 mV, respectively.

We know that the solution of this differential equation is

$$R_{th} = \Gamma_\infty + Ce^{\frac{-t}{\tau_{th}}}, \tag{2.25}$$

and C is determined by the initial condition in equation 2.24. In brief, after a spike is emitted, the threshold decays exponentially from Γ_0 toward Γ_∞ (see Figure 5A). In this model, Γ_0 was chosen to be a large, positive value because the authors intended to include the refractory period in this equation, that is, the threshold is so high after a spike that the neuron cannot fire. However, in the scenario where hundreds of synchronized excitatory spikes arrive, that is, the derivative of the membrane potential increases largely, even this threshold will be easily crossed. Therefore, this simplification has a limitation.

In Borisyuk's (2002) model, the threshold is expressed as

$$R_{th}(t+1) = (\gamma_{\max} - \gamma_\infty)\exp\left(\frac{-(t - t_{sp})}{\tau_{th}}\right) + \gamma_\infty, \tag{2.26}$$

where $\gamma_{\max} = -25$ mV and $\gamma_\infty = -55$ mV. Indeed, the threshold takes a maximum value $\gamma_{\max}$ when t, the current time, is equal to t^k; then it decays exponentially toward its asymptotic value γ_∞ (see Figure 5B). Meanwhile, the threshold equation is combined with a refractory process, that is, no

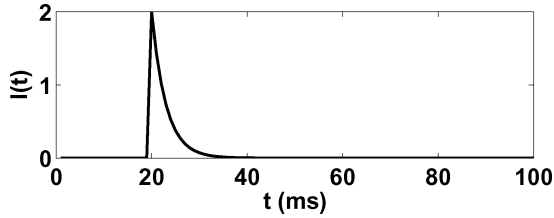

Figure 6: The decaying postsynaptic current when $\tau_s = 3$.

spikes can be generated from t^k to $t^k + \Delta$. From Figure 5, we can conclude that in both models, the threshold decays in the same way, except that the start and end values are different. The threshold in Borisyuk's model is more realistic, but the refractory period has to be taken into account. Other simplified neuron models have been used to explore the network dynamics; for example, noise and delay are not included in Tsodyks' model, and delay is ignored by Volman as well (Tsodyks, Uziel, & Markram, 2000; Volman, Baruchi, Persi, & Ben-Jacob, 2004).

3 Analysis in Discrete Time Domain

To implement an integrate-and-fire model, we first need to discretize the proper formulas or their solutions. Euler's method would be a good choice for discretizing the differential equations. However, since we have found the solutions analytically, computer calculations will be based on the solutions with each time step being equivalent to 1 ms in the neuronal network.

3.1 Postsynaptic Current/Potential. For the postsynaptic current, we choose the model described by equations 2.8 and 2.9. First, it is more realistic than the impulse mode (see Figure 1A); the current should decay gradually but not disappear instantly. Second, it can be implemented easily using the approach in equation 2.10, without inducing high computational expense as in the model in Figure 1C.

The decay constant τ_s is usually chosen to be small because the postsynaptic current decays very fast. For instance, when τ_s is 3, a spike of strength 2 arrives at $t = 20$ ms; the postsynaptic current is shown in Figure 6.

3.2 Membrane Potential. From section 2.2, we learned that in all integrate-and-fire models, the membrane potential has an exponentially decaying term (see equation 2.20). Essentially, if dominated by equation 2.14, the decaying term always goes to zero. Nevertheless, in the brain, the membrane decays toward the resting potential (about -70 mV), and the afferent spikes push the potential up to the threshold (-35 to -55 mV) for the next spike.

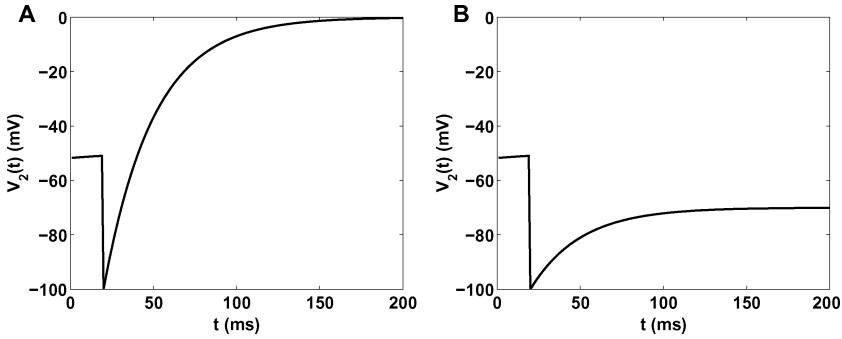

Figure 7: Two schemes for the decaying part of the membrane potential ($V_2(t)$). We assume that the decay constant τ_m is 30 and a spike is emitted at $t = 20$ ms. (A) The membrane potential decays toward zero. (B) It decays toward the resting potential (−70 mV).

In the discrete time model, if the membrane potential is chosen to decay toward zero, it will obey the following equation:

$$V_1(t) = \beta_m \exp\left(\frac{-(t - t^0)}{\tau_m}\right). \tag{3.1}$$

Otherwise, if we want it to decay toward the resting potential, the following equation has to be used:

$$V_1(t) = (\beta_m + 70)\exp\left(\frac{-(t - t^0)}{\tau_m}\right) - 70, \tag{3.2}$$

where β_m is the reset value of the membrane potential after a spike being generated and t^0 denotes the last spike time. These two schemes are shown in Figure 7.

In the approach where the membrane potential decays toward zero (see equation 3.1), it is certainly true that a neuron will fire at a fixed frequency without any incoming signal. And the fact that the membrane potential crosses the threshold while decaying makes the approach less plausible. However, in a model with thousands of neurons, spikes from the network will take effect well before the decaying term approaches the threshold. In that case, it would not matter if it decays toward the resting potential or zero. In our model, we will use equation 3.2 because it is also valid when we investigate the scenario in which spikes are rare.

The signal part of $V_m(t)$ is more complicated than the decaying part. In the simulations in Shen and De Wilde (2007), we used a clever simplification: we let the postsynaptic current be $V_2(t)$. This simplification is valid for

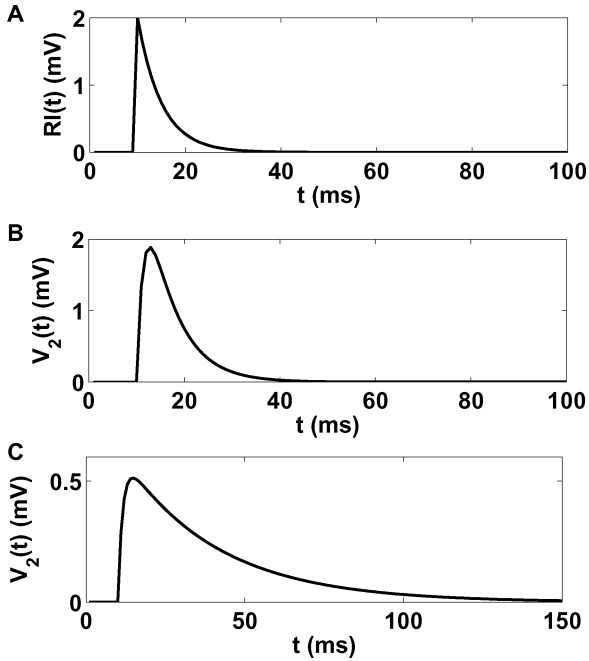

Figure 8: The shapes of the postsynaptic current and the signal part of the membrane potential. (A) A spike of strength 2 arrives at 10 ms, and the postsynaptic current decays exponentially ($\tau_s = 5$, $R = 1$). (B) With the same incoming spike, the plot of $V_2(t)$ in equation 2.21 shows a similar curve, except that this curve is smooth. Parameters are as follows: $R_m = 9$, $w_j = 2$, $\tau_s = 1.5$, and $\tau_m = 6$. (C) Plot of $V_2(t)$ when the membrane potential decay rate is chosen to be a more realistic value: $\tau_m = 30$. Other parameters remain the same.

simulating large-scale neuronal populations, provided that it is the macroscopic activity that we look at and that $I(t)$ and $V_2(t)$ have similar shapes (see Figure 8). We call this simplified model approach 1.

The curves in Figure 8 indicate that the decay constant τ_s has to be chosen from a different domain from that in approach 1 in order to obtain a similar decay rate. In addition, the membrane decay constant τ_m plays a role in the shape of $V_2(t)$ as well. For large τ_m, $V_2(t)$ climbs and decays very slowly, as $V_1(t)$ does. In other words, a single afferent spike will take effect for hundreds of milliseconds (see Figure 8C). This model will be referred to in the future as approach 2. If $V_2(t)$ in this approach is implemented following equation 2.21, it is obvious that a single spike's contribution to the membrane potential has to be taken into account to the very end of the simulation. In a long-term simulation with numerous spikes, there will be numerous equations, so the calculation is not feasible. That is the reason we

use equation 2.22: those two separate terms are constantly decaying, and each can be calculated in the following form:

$$V_{part}(t+1) = V_{part}(t)e^{\frac{-1}{\tau}}. \tag{3.3}$$

In other words, only the last value needs to be stored in the simulation. This makes long-term simulations with large neuronal populations possible.

Experiments have shown that the time constant of the membrane potential is typically between 20 ms and 50 ms. From Figure 8C, we can conclude that in approach 2, an incoming spike imposes a prolonged voltage increase on the membrane potential. The signal's magnitude stays above 50% of its maximum value for about 25 ms, and it takes approximately 100 ms for the signal to drop below 5% of its maximum value. This behavior raises an intriguing question: How can action potentials be emitted with 1 ms precision if the membrane potential changes so gradually? There has been no obvious answer to this question. However, we will demonstrate by simulations in the next sections that the network displays timing precision to some extent.

3.3 Summary of the Models. Based on the analysis above, we summarize the integrate-and-fire model that we will used.

For the postsynaptic current, we employ this equation:

$$I_{ij}(t+1) = I_{ij}(t)e^{\frac{-1}{\tau_s}} + \alpha, \tag{3.4}$$
$$\alpha = \begin{cases} w_{ij} & \text{if } t+1 = t_j^k + \Delta t_{ij} \\ 0 & \text{else,} \end{cases}$$

where w_{ij} is the synaptic weight from neuron j to neuron i, t_j^k denotes the last spike time of neuron j, and Δt_{ij} is the axonal conduction delay from j to i.

The membrane potential consists of two parts. The decaying part is

$$V_1(t) = (\beta_m + 70)e^{\frac{-(t-t^k)}{\tau_m}} - 70, \tag{3.5}$$

where β_m is the reset value of the membrane potential after a spike being generated, and t^k denotes the last spike time.

For the signal part of the membrane potential, there are two approaches. In approach 1,

$$V_2(t) = R_m \times \sum_j I_j(t), \tag{3.6}$$

where R_m is just 1 because the magnitude of the signal is already represented by the synaptic weight. In approach 2,

$$\begin{aligned} V_{2a}(t+1) &= V_{2a}(t)e^{\frac{-1}{\tau_s}} + \alpha, \\ V_{2b}(t+1) &= V_{2b}(t)e^{\frac{-1}{\tau_m}} + \alpha, \\ V_2(t+1) &= V_{2a}(t+1) - V_{2b}(t+1). \end{aligned} \tag{3.7}$$

$$\alpha = \begin{cases} \dfrac{w_{ij}R_m}{\tau_s - \tau_m} & \text{if } t+1 = t_j^k + \Delta t_{ij} \\ 0 & \text{else.} \end{cases}$$

And finally, the threshold is defined by

$$R_{th}(t+1) = (\gamma_{\max} - \gamma_\infty)e^{\frac{-(t-t^k)}{\tau_{th}}} + \gamma_\infty, \tag{3.8}$$

where $\gamma_{\max}$ is the reset value after a spike and γ_∞ is the asymptotic value that the threshold decays to.

All simulations in the following sections are based on this model. We specify if we use approach 1 or approach 2 for each particular simulation.

4 Oscillations and Spiking Pairs

The notion of oscillation represents a macroscopic behavior in which neurons discharge together in one time frame and are silent in another. The typical oscillatory activity of the neuronal population can be observed in Figure 10A. In our previous studies (Shen & De Wilde, 2007), we found that oscillations persist while parameters such as the connection ratio and the synaptic strength vary in wide ranges. For instance, regular oscillations exist when the mean synaptic strength is in (0.8, 10) when other parameters remain the same. Furthermore, the value of any parameter affects other parameters' ranges.

It is true that oscillatory activities have been confirmed to be important properties of neuronal populations. Nevertheless, it conceals the microscopic aspect of the firing pattern: spike timing precision. Izhikevich (2006) investigated spike timing precision in terms of neuronal groups. In our research, we emphasize the more basic units: causal spiking pairs.

We call neurons A and B a causal spiking pair if they satisfy these conditions:

1. A is an excitatory neuron, and there is a synapse from A to B.
2. In the simulation time, it occurred at least N_α times that B fires exactly τ_α ms after A fires.
3. τ_α is not less than the axonal conduction delay from A to B,Δt_{ab} but also not greater than $\Delta t_{ab} + T_\alpha$.

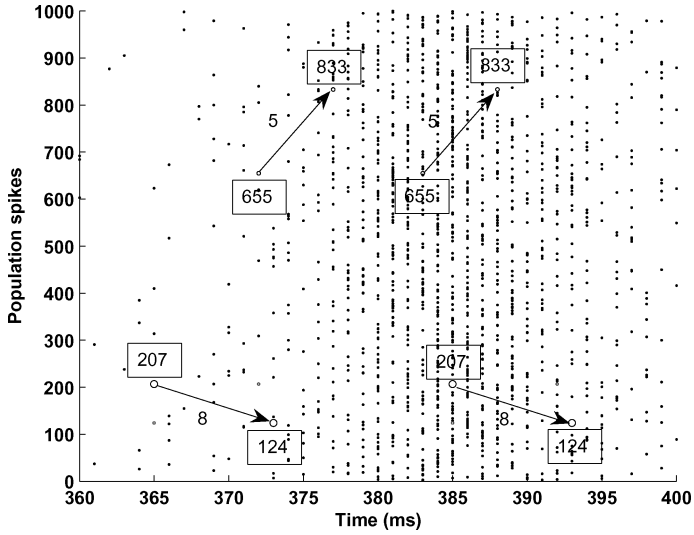

Figure 9: Part of the spike map of 1000 neurons in a 1000 ms simulation. Circles are spikes of interest, and dots represent all other spikes. The labels of the neurons in these two pairs are written in boxes, and the numbers along arrows are axonal conduction delays.

The values of parameters N_α and T_α should be chosen according to the model and simulation length. Essentially N_α sets up the minimum number of occurrences for the pairs. Meanwhile, since the postsynaptic current decays exponentially, T_α ensures that the presynaptic neuron's contribution to the postsynaptic neuron is significant, that is, there is a causal relation between the two spikes. Two examples of spiking pairs are shown in Figure 9.

4.1 Approach 1. Here we use approach 1, described in section 3.3 as the neuronal model, and simulate 1000 interconnected neurons. A noise term is defined as

$$N(t+1) = N(t)\exp\left(\frac{-1}{\tau_N}\right) + \xi, \quad \xi \epsilon N(0,\sigma), \tag{4.1}$$

which is added to the membrane potential. All parameters are summarized in Table 1, and they are uniformly distributed around their mean values with some standard deviation, so randomness is included in every neuron's properties. All of these values are chosen according to experimental data (Shadlen & Newsome, 1998) and previous models (Borisyuk, 2002; Iglesias, Eriksson, Grize, Tomassini, & Villa, 2005). To reduce the complexity of the system, we minimized the difference between excitatory and inhibitory

Table 1: Default Parameters in the Investigation.

	Excitatory Neurons		Inhibitory Neurons	
Parameter	*Mean*	*SD*	*Mean*	*SD*
$\gamma_{\max}$ (mV)	−25.0	5.0	−25.0	5.0
γ_{∞} (mV)	−55.0	3.0	−55.0	3.0
τ_{th}	3.0	1.0	10.0	2.0
τ_N	5.0	0.5	5.0	0.5
τ_m	30.0	1.0	30.0	1.0
σ (mV)	5.0	0.5	5.0	0.5
β_m (mV)	−100.0	2.0	−100.0	2.0
t_{ref} (ms)	3.0	1.0	3.0	1.0
w^{ij}	1.8	0.18	−3.2	0.32
τ_s	2.0	0.4	6.0	1.2
Δt_{ij}	4.0	2.0	4.0	2.0

neurons: there are only three parameters (τ_{th}, w^{ij}, and τ_s^{ij}) that differentiate excitatory and inhibitory neurons.

Oscillations are robust against fluctuations in these parameters. Figure 10 shows that salient oscillations in beta range (10–30 Hz) emerge from the network. Meanwhile, excitatory and inhibitory spikes achieve good balance throughout the course of the simulation. No saturation has occurred, and all neurons discharge at reasonable rates. Figure 10 also shows that although the whole network exhibits oscillations at low frequency, neurons may fire two to four times in a bursting cycle. Calculations suggest that on average, each neuron emitted 39.53 spikes in a 1000 ms simulation.

We searched for spiking pairs in the duration from 101 ms to 900 ms and found exactly 8775 spiking pairs in the above simulation. The search was not from 0 ms because the first few spikes of the population may be affected by the initial state of the network, while after 100 ms, the oscillatory activity appeared fairly regular. In this search, N_α was 12 and T_α was 1. In other words, the criteria of spiking pairs were as follows. First, they appeared at least 12 times; second, the time intervals between the two neurons' spikes had to be either Δt_{ij} (the conduction delay) or $\Delta t_{ij} + 1$. Note that there were only 12 bursting cycles between 100 ms and 900 ms in the simulation (see Figure 10A), which means that on average, each spiking pair should have at least one occurrence in a cycle. In addition, because in approach 1 the postsynaptic current decays rapidly, we chose T_α to be small to make sure the presynaptic neuron contributes significantly to the firing of the postsynaptic neuron. These spiking pairs are recorded in Table 2.

Figure 11 illustrates some characteristics of these spiking pairs. We notice that the conduction delays in spiking pairs follow an approximate normal distribution (see Figure 11A) although for all synapses, they follow a uniform distribution. This implies that spiking pairs have a bias toward pairs

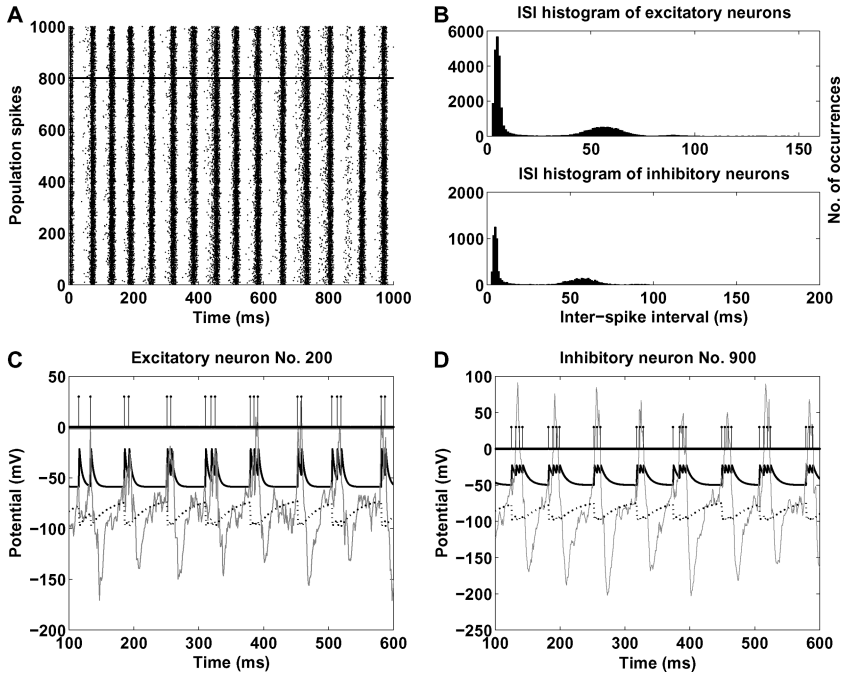

Figure 10: Oscillations for approach 1: (A) Scatter plot of all the spikes. Each dot represents a spike; below the solid line are excitatory neurons' spikes, and above the line are inhibitory spikes. (B) Histograms of interspike intervals for both excitatory and inhibitory populations. (C) Plot of the internal activity of a typical excitatory neuron. Vertical lines represent spikes; the threshold is the black solid line, and the gray line and the dotted line denote the signal part and the decaying part of the membrane potential, respectively. (D) Plot of the internal activity of a typical inhibitory neuron.

that have average conduction delays. The number of times that a spiking pair appears, on the other hand, follows roughly a power law distribution (see Figure 11B). We conclude that in all these spiking pairs, most occurred 12 or 13 times, or approximately once in a bursting cycle. However, a small number of pairs were able to fire several times in a bursting cycle.

4.2 Approach 2. Using approach 2, we simulated this network again and also found oscillatory behavior. The parameters specifically modified for approach 2 are listed in Table 3. All other parameters remained the same.

Note that the parameter R_m, together with τ_s, τ_m, and w_{ij}, controls the magnitude of the signal part of the membrane potential (see equation 3.7). Although R_m is a property of the membrane of the cell, it does not need

Table 2: Spiking Pairs.

Presynaptic Neuron Number	Postsynaptic Neuron Number	Number of Occurrences	Delay
1	59	12	4
1	318	12	4
1	333	14	5
1	353	12	6
1	669	13	5
2	559	12	6
4	95	13	5
⋮	⋮	⋮	⋮
669	4	13	5
669	39	13	4
⋮	⋮	⋮	⋮
799	381	12	2

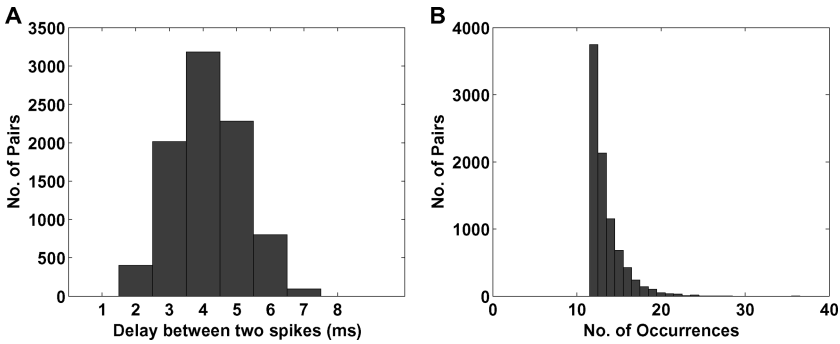

Figure 11: Properties of the spiking pairs for approach 1. (A) Distribution of the delays between spikes in all spiking pairs: we sort all the spiking pairs according to the delay between the presynaptic and postsynaptic spikes. (B) Distribution of the number of occurrences in all spiking pairs: we sort all the spiking pairs according to the number of their occurrences.

Table 3: Parameters for Approach 2.

	Excitatory Neurons		Inhibitory Neurons	
Parameter	*Mean*	*SD*	*Mean*	*SD*
w^{ij}	1.8	0.18	−7.6	0.76
τ_s	1.5	0.3	15.0	3.0
R_m	5.0	0.0	5.0	0.0

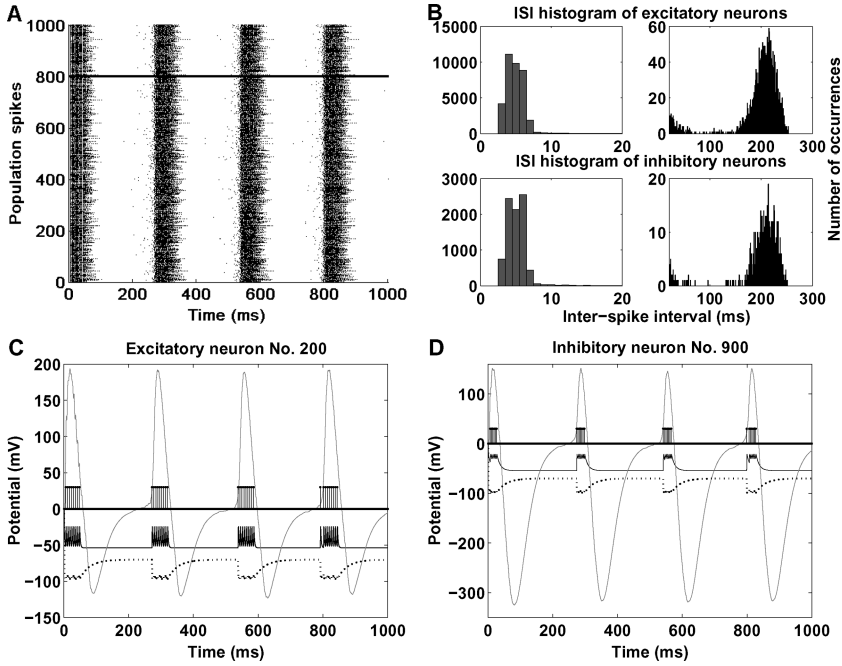

Figure 12: Saturated oscillations for approach 2 ($R_m = 5$). (A) Scatter plot of all the spikes. Each dot represents a spike; below the solid line are excitatory neurons' spikes, and above the line are inhibitory spikes. (B) Histograms of interspike intervals for both excitatory and inhibitory populations. Each histogram is divided into two sections (0–20 ms and 20–300 ms) in order to show the peak around 200 ms. (C) Plot of the internal activity of a typical excitatory neuron. The meaning of each type of line is same as in Figure 10. (D) Plot of the internal activity of a typical inhibitory neuron.

to follow a certain distribution, because the uniqueness of a neuron has already been well represented by τ_s and τ_m.

These parameters are chosen for the purpose of achieving balanced excitatory and inhibitory spikes. In section 3.2, we showed that the voltage on the membrane potential ($V_2(t)$) imposed by an incoming spike lasts a long time. In order to balance with the long-lasting positive voltage caused by 800 excitatory neurons, the weights of the inhibitory synapses have to be greater and their decay rates have to be slower than in approach 1. We also find that oscillations are not so robust against changes in parameters as in approach 1. Both w_{ij} and τ_s have to be carefully chosen; otherwise the whole network could easily end up in the scenarios where all neurons fire as rapidly as possible or all neurons stop firing.

We observe two types of oscillatory behavior when only R_m is adjusted. The first type ($R_m = 5$) is shown in Figure 12, in which there were only a

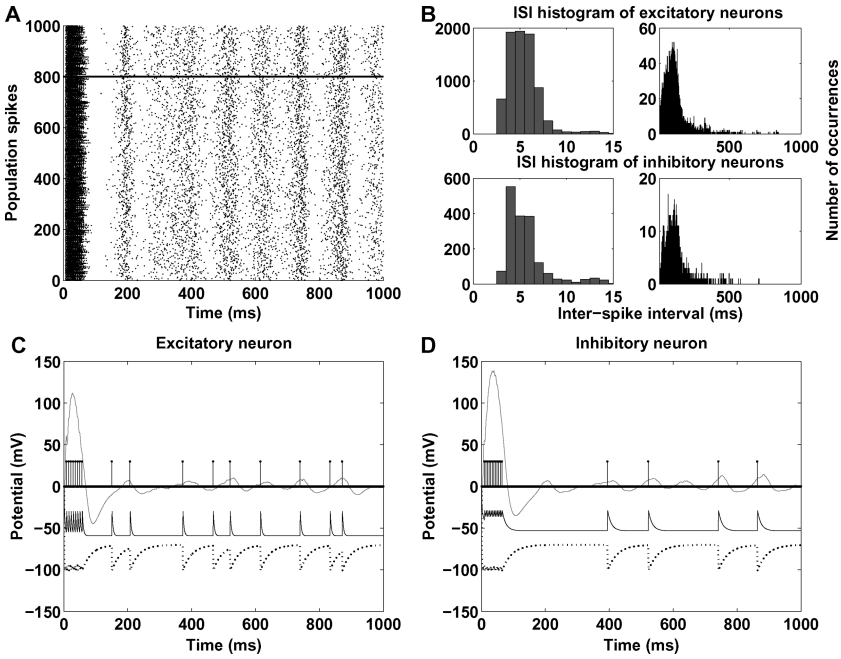

Figure 13: The obscure oscillation for approach 2 ($R_m = 3$). (A) Scatter plot of all the spikes. (B) Histograms of interspike intervals in both excitatory and inhibitory populations. (C) Plot of the internal activity of a typical excitatory neuron. (D) Plot of the internal activity of a typical inhibitory neuron.

few bursting cycles in the 1000 ms simulation. Each neuron fired several times closely, because the signal part of the membrane potential changed very smoothly and kept the total potential well above the threshold for tens of milliseconds; thus, only the refractory period was controlling the spike rate. This type of oscillation is called *saturated oscillation*. When R_m was changed to 3, we found the second type of oscillation. The oscillatory activity was less salient and regular (see Figure 13), so we call it *obscure oscillation*. From Figures 13C and 13D, we can see that the signal part of the membrane potential is usually not strong enough to push the total potential across the threshold. This implies that noise makes some contribution to the firing of the neurons.

In the saturated oscillation, the average firing rate of a neuron is 48.46 spikes per second, while in the obscure oscillation, the average rate is 16.23 spikes per second. And more interesting, although the spike rates are very different in these two types of oscillations, the distribution of interspike intervals stays very similar (see Figures 12B and 13B). The majority of the intervals are between 4 ms and 8 ms, which implies that

even in the obscure oscillation, it is very common that a neuron fires close spikes.

From a neurophysiological point of view, the obscure oscillation is more plausible because the neuronal activity is very sensitive to the input from outside. The signal part of the membrane potential fluctuates periodically with the frequency being around 10 Hz, but the amplitude is not high enough to cause the neuron to fire. Therefore, if the peak of the membrane potential coincides with some excitatory external input, a spike will be emitted. Essentially the internal oscillatory activity of the network provides a mechanism in which inputs from outside can be modulated. With completely random input, we observe that the network as a whole oscillates at a slightly lower frequency (about 10 Hz) than an average single neuron does (16 Hz). Because of its sensitivity, the neuronal behavior will be different when there is stimulus. Both the spike rate and spike timing will be adjusted according to the stimulus, and of course, this adjustment is subject to the internal modulation.

Before searching for spiking pairs in these simulations, we need to set a new value for T_α. In the previous simulations with approach 1, T_α was only 1 because the signal from a presynaptic neuron to a postsynaptic neuron decreases very fast. In approach 2, on the contrary, the signal increases sharply and then decreases slowly. This implies that the contribution from a presynaptic spike is significant for tens of milliseconds. Hence, the delay between a presynaptic spike and a postsynaptic spike ought to be considered in a wide range when we search for causal spiking pairs.

With the search criteria $N_\alpha = 36$ and $T_\alpha = 50$, 2042 spiking pairs were found in the saturated oscillation. This indicates that 2042 spiking pairs occurred at least 36 times within 800 ms. From Figure 14B, we can see that about 400 pairs occurred exactly 36 times. As the number of occurrences declines, the number of pairs increases exponentially. In like manner, if the number of occurrences becomes greater, the number of pairs decreases exponentially. We did not calculate the pairs that occurred fewer than 36 times because the number would be large and it would be very time-consuming. The fact that the number of spiking pairs is really large is to be expected because every neuron fired consecutively in a bursting cycle, and thus there were many possible pairs; in addition, a bursting event lasted almost 100 ms, so each pair might occur tens of times in the event.

In contrast, with the obscure oscillation, there were only 960 spiking pairs that occurred more than twice. More precisely, 937 spiking pairs occurred three times and 23 pairs occurred four times (see Figures 14C and 14D). Although these data were gathered from one simulation, simulating the network multiple times confirms that the number of spiking pairs that occur three times or more is on the same scale as the number of neurons in this kind of network. In comparison with the distribution of delays in Figure 11, the delays between spikes in pairs come from a wider range (see Figure 14C). This again is because the signal part of the membrane potential

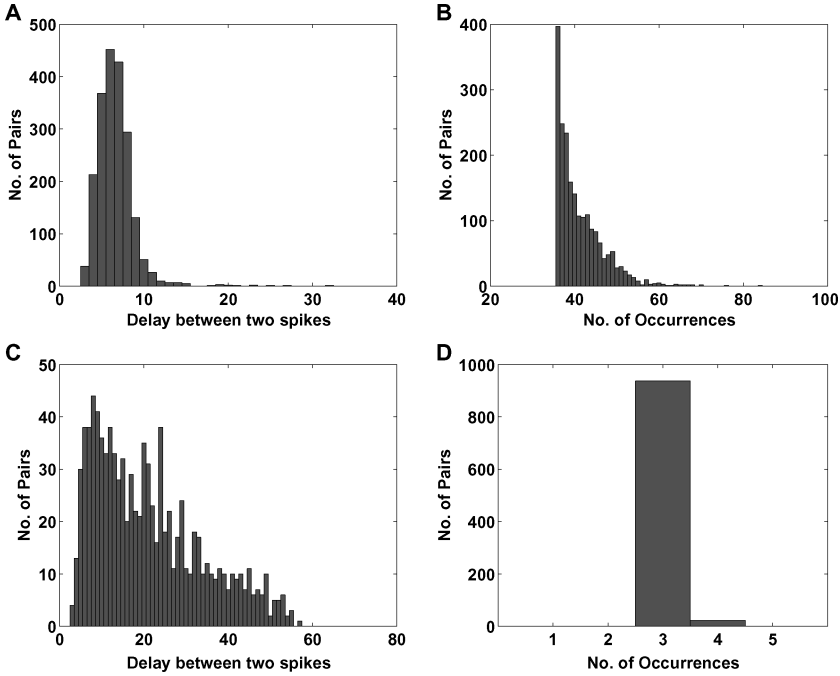

Figure 14: Properties of the spiking pairs with approach 2. (A) Distribution of the delays between spikes in all spiking pairs in the saturated oscillation with approach 2. (B) Distribution of the number of occurrences in all spiking pairs in the saturated oscillation. (C) Distribution of the delays between spikes in all spiking pairs in the obscure oscillation. (D) Distribution of the number of occurrences in all spiking pairs in the obscure oscillation.

decays really slowly. The large variance in the delays among spiking pairs is in line with the results from neurophysiological experiments (Shadlen & Newsome, 1998), in which the variance of interspike intervals is also large. In terms of both oscillations and spiking pairs, the obscure oscillation is more plausible than the saturated oscillation.

4.3 Consequences. The notion of spike timing precision is based on the fact that the exact timing of a group of neurons is reproducible. The sizes of these groups could vary, but all consist of one or several spiking pairs. In Table 2, for example, we list all the spiking pairs that meet the criteria in that simulation. Neuron 1 and neuron 669 form a pair, and neuron 669 and neuron 39 are also a pair; therefore, these three neurons all belong to a firing group of three (see Figure 15A). As we search the table of spiking pairs, we may find larger groups (see Figure 15B). Although it is likely that

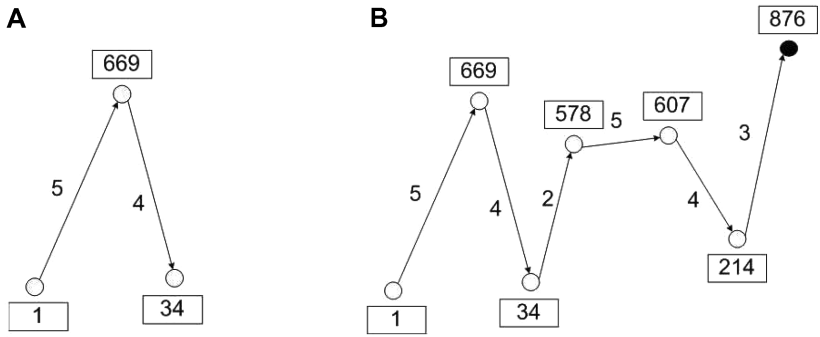

Figure 15: Spike timing groups. (A) A firing group of three. (B) The firing group of three actually belongs to a bigger group with an inhibitory neuron at the end of the sequence.

the groups may not occur as many times as the individual pairs (e.g., there may be times when neuron 1 fired and then neuron 669 fired but neuron 39 did not follow), the number of spiking pairs does suggest how many neuronal groups there potentially are, and thus how precise in timing the network is.

5 Neuronal Model with STDP Algorithms

Spike-timing-dependent plasticity (STDP) has been extensively studied in neural models recently (Song et al., 2000). The spike timing correlation between presynaptic and postsynaptic neurons determines potentiation or depression of synapses (Bi & Poo, 2001). Essentially it is a simple algorithm for changing synaptic strengths that has been experimentally observed in the brain (Dan & Poo, 2004). In this section, we investigate the behavior of the neuronal network coupled with STDP learning algorithms in terms of oscillations and spike timing precision.

5.1 Spike-Timing-Dependent Plasticity. The standard STDP modification function can be found in Figure 16A. The percentage change of the synaptic weight is determined by the time delay between the pre- and postsynaptic spikes. In our simulations, we apply the same function except that the change in strength is denoted by the actual value but not the percentage (see Figure 16B). This simplification is used because we want to control the weights within a certain limit. It is obvious that with the scheme in Figure 16A, strong connections will easily become stronger and stronger, and the network will end up in a state dominated by a small number of strong connections.

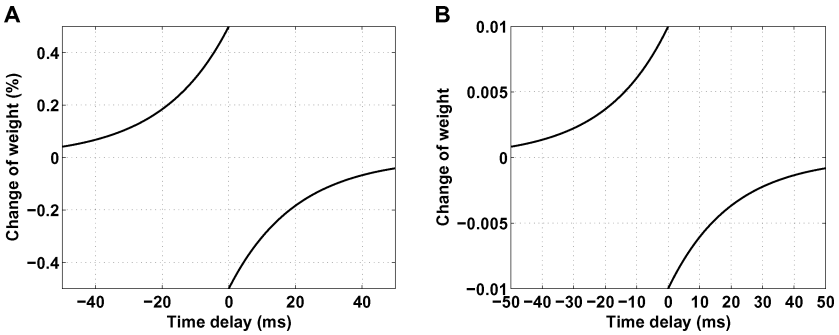

Figure 16: (A) Theoretical STDP modification function. (B) The STDP function we use in our simulations.

The mathematical description of STDP is given by

$$F(t_\Theta) = \begin{cases} A_+ \exp(t_\Theta/\tau_+) & \text{if } t_\Theta < 0 \\ -A_- \exp(-t_\Theta/\tau_-) & \text{if } t_\Theta > 0, \end{cases} \tag{5.1}$$

where t_Θ is the time delay between the pre- and postsynaptic spikes. A_+ and A_- are parameters that represent the maximum change, and τ_+ and τ_- are parameters that denote the decay rate of the function. The typical values of these parameters are $A_+ = A_- = 0.005$, $\tau_+ = \tau_- = 20$ ms. In our simulations, we use the same equation; the only difference is that A_+ and A_- are 0.01 and that they mean the actual change of weights (see Figure 16B).

Theoretically the STDP function should be applied to any pair of pre- and postsynaptic spikes. However, that is unfeasible and unnecessary. Suppose there are N neurons in a simulation of length T ms; the total number of spikes will be on the order of $N \times T$. Therefore, the total number of pairs of spikes that we need to apply the STDP function to will be on the order of $N^2 \times T^2$. This induces high computational expenses. Moreover, from the STDP function in Figure 16, we know that the change of weights is tiny when the delay between two spikes is large. Consequently, the network can be simulated in good approximation, even if we compute only the pairs that are close together in time. In some studies, STDP is implemented by considering only nearest-neighbor spikes (Izhikevich & Desai, 2003). In our simulations, we open a window of 50 ms for computing the STDP function, in other words, spikes that are more than 50 ms away from each other are not considered. In fact, the graph in Figure 16B represents the actual size of the STDP window that we are using. This process is very easy to implement in the simulations: whenever a spike is generated, we

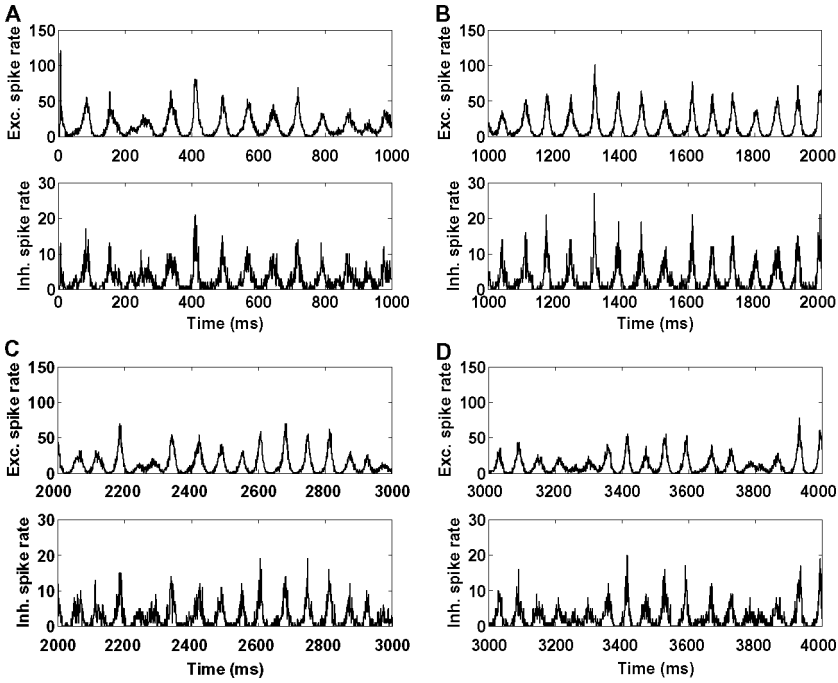

Figure 17: Spike rates of neurons at different times in a 4000 ms simulation with STDP learning algorithms. (A) Excitatory and inhibitory spike rates in the first 1000 ms. (B) Excitatory and inhibitory spike rates from 1001 ms to 2000 ms. (C) Excitatory and inhibitory spike rates in the third 1000 ms. (D) Excitatory and inhibitory spike rates from 3001 ms to 4000 ms.

just look back 50 ms, find all the related spikes, and change the weights accordingly.

5.2 Behavior of the Network with STDP. The neuronal model used here is the same as that in section 4.1. However, the simulation length here is set to 4000 ms. For the first 1000 ms, the STDP learning is not applied, so the network just behaves according to its intrinsic properties. From 1001 ms to 3000 ms, the STDP algorithm functions and modifies the synaptic weights. After 3000 ms, STDP is removed again, so the network is operating with the new fixed weights.

The spike rate of the neuronal population in each 1000 ms can be found in Figure 17. We can conclude that the network still oscillates with STDP learning introduced. However, as the STDP function operates longer, the period gradually changes and the oscillations become less regular. Calculations suggested that the identified periods were 77 ms, 69 ms, 63 ms,

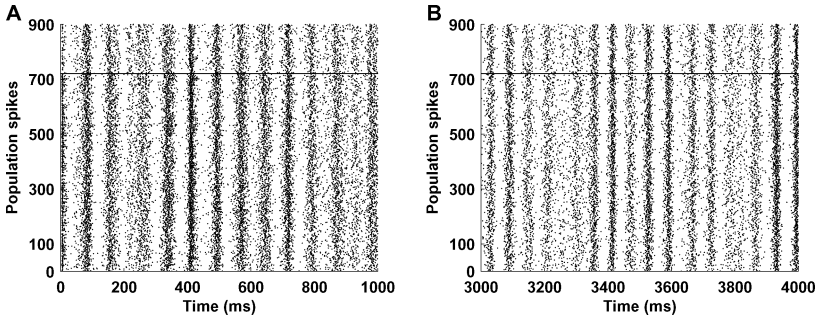

Figure 18: Plots of the spikes in the simulation with STDP function. (A) Scatter plot of all the spikes from 1 ms to 1000 ms; below the solid line are excitatory spikes, and above the line are inhibitory spikes. (B) The same plot from 3001 ms to 4000 ms.

and 52 ms in the first, second, third, and fourth 1000 ms of the simulation, respectively. We know that once the parameters of the network are determined, oscillations exhibit a stable period. Therefore, the periods calculated in the first and last 1000 ms reflect the oscillatory properties of the network. The network must be in a transient state between 1000 ms and 3000 ms, in which the period was changing because the weights were constantly being modified. The coefficient of oscillation was 2.39 in the first 1000 ms and 1.62 in the last, indicating the level of regularity of oscillation was reduced. We also plot all the spikes in the first and last 1000 ms (see Figure 18), in which a change of period can be easily observed.

When we discussed the oscillatory behavior of approach 1 in section 4, we argued that it is very common for one neuron to fire a few close spikes in a bursting cycle. This fact is well reflected by the peaks between 1 ms and 10 ms in the distribution of interspike intervals (see Figure 10B). In the simulation here, the histogram of the interspike intervals without STDP learning is shown in Figure 19A. Compared with the simulation in Figure 10(B), two parameters are different here. The first is the mean axonal delay, which has been changed to 10 ms from 3 ms; the second parameter is the standard deviation of noise, which has been increased from 5.0 to 6.0. Obviously the change of the distribution of interspike intervals is mainly attributed to the increase of axonal delays. Nevertheless, longer axonal conduction delays only reduce the magnitude of the first peak in the histogram. There are still two humps in the distribution before STDP starts to function (see Figure 19A). As the simulation proceeds, the first hump shrinks, while the second hump gradually shifts its peak from above 70 ms to about 50 ms (see Figures 19B to 19D). This is in line with our observation of the period change. All of the results above suggest that significant modulations on the oscillation of neuronal populations arise from the STDP

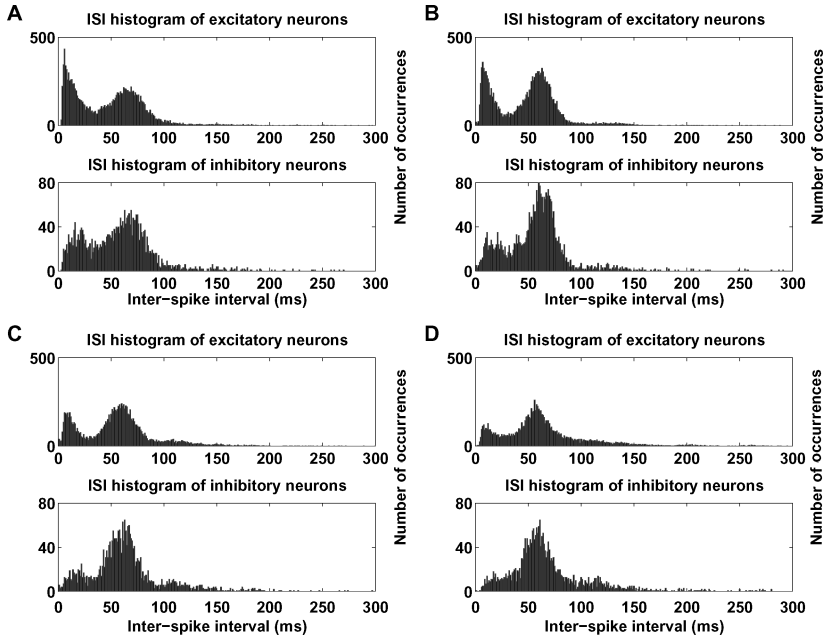

Figure 19: Distribution of interspike intervals at different times. (A) T = 1000 ms. (B) T = 2000 ms. (C) T = 3000 ms. (D) T = 4000 ms.

learning algorithm. On the one hand, it modifies the frequency of the oscillation. And on the other hand, it prevents many neurons from firing spikes consecutively.

The STDP algorithm applies to each of the connections between neurons. A potential outcome of these individual operations is the overall distribution of the weights being fundamentally altered. In our simulations, we observed that all of the synaptic connections had been modified and that the distribution of the weights tended to transform into a normal distribution (see Figure 20). More simulations confirm that as STDP modification lasts longer, the range of the synaptic weights becomes wider and the distribution becomes more bell shaped.

It is realistic to set up boundaries for the weights because the efficacy of a synapse cannot be arbitrary. This was not necessary in the above simulation because no weight had gone beyond the reasonable range. However, if we apply the STDP algorithm long enough, boundaries might be required and the distribution could be different with the presence of boundaries. In the long-term simulation with 20000 ms of STDP, the synaptic weights remained bell shaped and restricted within $(-10,10)$. Therefore, in our study, we assume that no boundaries are needed for synaptic weights.

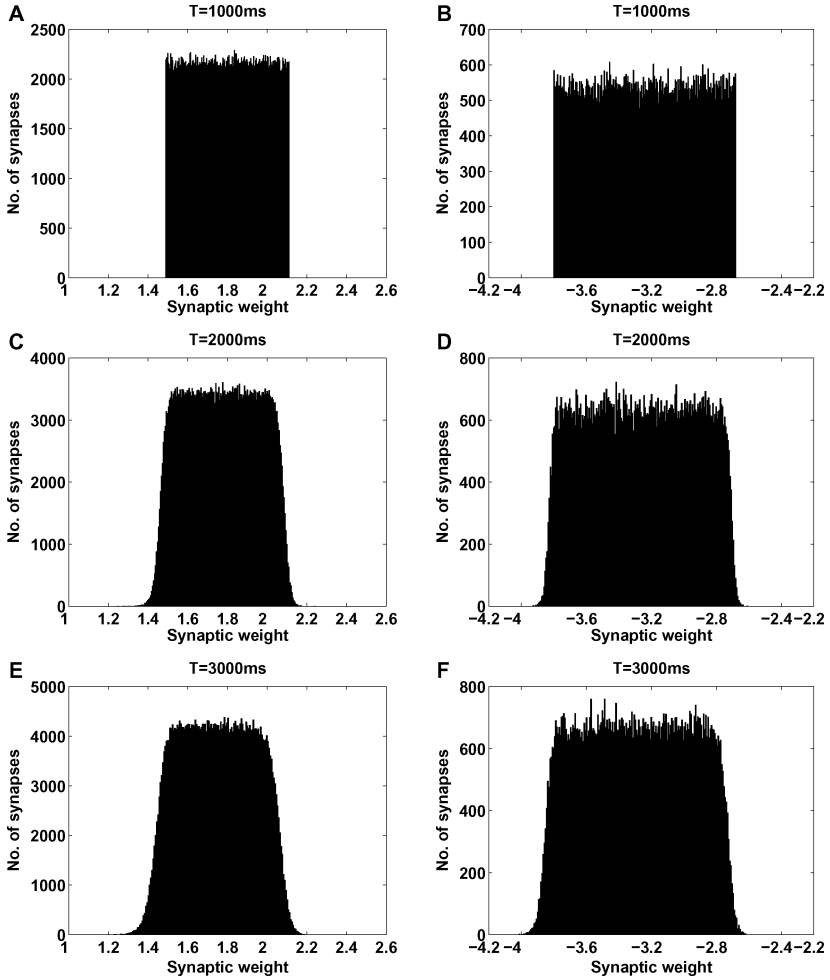

Figure 20: Distribution of the excitatory and inhibitory synaptic weights at different times. (A) Excitatory, T = 1000 ms. (B) Inhibitory, T = 1000 ms. (C) Excitatory, T = 2000 ms. (D) Inhibitory, T = 2000 ms. (E) Excitatory, T = 3000 ms. (F) Inhibitory, T = 3000 ms.

Intuitively, we suppose that the number of spiking pairs will be increased by the STDP algorithm, because STDP simply encourages neurons to fire at the "right time." However, the simulations say the contrary. In the above simulation, there were 1988 spiking pairs found in the first 1000 ms, during which the STDP function was not included. In the second and third 1000 ms with STDP, the numbers of pairs were 1481 and 447, respectively. And

in the last 1000 ms in which the STDP function had been removed, only 363 spike pairs were found. The search criteria were exactly the same: we used only the 800 ms in the middle of the 1000 ms window, $N_\alpha = 4$ and $T_\alpha = 1$.

6 Conclusion and Discussion

6.1 Oscillations and Spiking Pairs in Two Integrate-and-Fire Schemes. From the overview of different integrate-and-fire models, we conclude that there are two different approaches concerning the postsynaptic current: fast decaying (approach 1) and slow decaying (approach 2). But the schemes for the membrane potential and the threshold in the literature are all somewhat convergent. Oscillations were observed for both approaches 1 and 2. The difference is that for approach 2, oscillations are not so robust against fluctuations in parameters as for approach 1. The slow-decaying postsynaptic current prolongs the period of oscillations and makes oscillations less robust. However, when the oscillatory activity is more sensitive, potentially it can convey information more easily. Since the neuronal population in our simulations is an autonomous system, the results regarding robustness and sensitivity will provide a good reference for future investigations with stimuli or coded input signals.

We also defined the notion of spiking pair as a measure of the spike timing precision in neuronal firing patterns. A spiking pair is two neurons repeatedly firing in a causal relation. It is the fundamental unit in spiking clusters that have been confirmed to exist in the brain. Hence, the number of spiking pairs reflects how precise in timing the network is. Simulations indicated that spiking pairs exist for both approaches 1 and 2. The number of spiking pairs detected increased exponentially as we lowered the repeated time barrier, suggesting that it was very common for a pair of neurons to repeat their firing sequence several times in a 1000 ms simulation. The emergence of pairs or groups with casual firing relations expresses the microscopic aspect of the firing pattern. It also supports the hypothesis that information is coded in neuronal clusters repeatedly firing with time precision.

6.2 Effects of STDP Algorithm. According to the timing of pre- and postsynaptic neurons, the STDP algorithm modifies the synaptic strengths permanently, and it acts as a learning mechanism in the neuronal population. The STDP learning algorithm accelerated the oscillation while decreasing the number of spiking pairs.

The distribution of synaptic weights was initially uniform, and the STDP learning algorithm gradually changed it to a normal distribution. This has a profound impact on the oscillatory behavior of the network. The frequency could be increased by 30% after several seconds of STDP learning. We already know that the frequency is sensitive to the mean synaptic strength

(Shen & De Wilde, 2007). Hence, when information is being processed in the brain, the period of oscillations is modulated by changes in both the mean value and the distribution of synaptic strengths, and these changes are caused by STDP functions.

6.3 Uncertainty in Neuronal Populations. The neuronal basis of uncertainty in the brain is the irregularity of firing. This can be interpreted from several perspectives. First at no time is one neuron going to fire for certain. The probability of firing can be high or low but cannot be 1. In our models, this uncertainty is present because of the existence of noise. Noise could neutralize the incoming positive voltage and thus prevent the firing. Second, the variance of the interspike intervals is large. Essentially the interspike intervals vary partly because every neuron fires in a stochastic manner. Meanwhile, our simulations implicate that axonal conduction delays being in a wider range, and the STDP learning algorithm also increases the variance of the interspike intervals. When we change our perspective from individual neurons to pairs of neurons, the notions of timing relation and reproducibility arise. When most of the pairs discharge with fixed delays repeatedly, the population obviously conveys little information and will not be sensitive to the stimulus from outside. Our simulations with realistic parameters suggest a possible regime in which spike timing precision is present. The reoccurrence of the spiking pairs represents the level of precision, and the standard deviation reflects uncertainty. It is also suggested by simulations that the STDP function affects the behavior of spiking pairs. When the view is broadened to neuronal populations, the main focus is on oscillations. The period of the oscillation is still uncertain mainly because STDP regulates the period, and STDP is based on spike timing, which is uncertain. However, the overall oscillatory activity is controlled by the collective interactions among neurons, astrocytes, and the STDP algorithm. The modeling and simulation of those collective interactions, including the astrocytes, is the subject of current work.

References

Amit, D., & Brunel, N. (1997). Model of global spontaneous activity and local structured activity during delay periods in the cerebral cortex. *Cerebral Cortex*, *6*, 237–252.

Beggs, J. M., & Plenz, D. (2004). Neuronal avalanches are diverse and precise activity patterns that are stable for many hours in cortical slice cultures. *Journal of Neuroscience*, *24*, 5216–5229.

Bi, G. Q., & Poo, M. M. (2001). Synaptic modification by correlated activity: Hebb's postulate revisited. *Annual Review of Neuroscience*, *24*, 139–166.

Bliss, T. V., & Gardner-Medwin, A. R. (1973). Long-lasting potentiation of synaptic transmission in the dentate area of the unanaesthetized rabbit following stimulation of the perforant path. *Journal of Physiology*, *232*, 357–374.

Bliss, T. V., & Lømo, T. (1973). Long-lasting potentiation of synaptic transmission in the dentate area of the anaesthetized rabbit following stimulation of the perforant path. *Journal of Physiology*, *232*, 331–356.

Borisyuk, R. (2002). Oscillatory activity in the neural networks of spiking elements. *BioSystems*, *67*, 3–16.

Brunel, N., & Hakim, V. (1999). Fast global oscillations in networks of intergrate-and-fire neurons with low firing rates. *Neural Computation*, *11*, 1621–1671.

Coombes, S. (2003). Dynamics of synaptically coupled integrate-and-fire-or-burst neurons. *Physical Review E*, *67*, 041910–1–9.

Dan, Y., & Poo, M. (2004). Spike timing–dependent plasticity of neural circuits. *Neuron*, *44*, 23–30.

Giudice, P. D., Fusi, S., & Mattia, M. (2003). Modelling the formation of working memory with networks of intergrate-and-fire neurons connected by plastic synapses. *Journal of Physiology, Paris*, *97*, 659–681.

Iglesias, J., Eriksson, J., Grize, F., Tomassini, M., & Villa, A. (2005). Dynamics of pruning in simulated large-scale spiking neural networks. *Biosystems*, *79*, 11–20.

Izhikevich, E. (2006). Polychronization: Computation with spikes. *Neural Computation*, *18*, 245–282.

Izhikevich, E. M., & Desai, N. S. (2003). Relating STDP to BCM. *Neural Computation*, *15*, 1511–1523.

Kelso, S. R., & Brown, T. H. (1986). Differential conditioning of associative synaptic enhancement in hippocampal brain slices. *Science*, *232*, 85–87.

Kreiter, A., & Singer, W. (1996). Stimulus-dependent synchronization of neuronal responses in the visual cortex of the awake macaque monkey. *Journal of Neuroscience*, *16*, 2381–2396.

Mainen, Z. F., & Sejnowski, T. J. (1995). Reliability of spike timing in neocortical neurons. *Science*, *268*, 1503–1506.

Melamed, O., Silberberg, G., Markram, H., Gerstner, W., & Richardson, M. (2005). Subthreshold cross-correlations between cortical neurons: A reference model with static synapses. *Neurocomputing*, *65–66*, 685–690.

Panchev, C., & Wermter, S. (2004). Spike-timing-dependent synaptic plasticity: From single spikes to spike trains. *Neurocomputing*, *58–60*, 365–371.

Reinagel, P., & Reid, R. C. (2000). Temporal coding of visual information in the thalamus. *Journal of Neuroscience*, *20*, 5392–5400.

Segev, R., Baruchi, I., Hulata, E., & Ben-Jacob E. (2004). Hidden neuronal correlations in cultured networks. *Physical Review Letters*, *92*, 102–105.

Shadlen, M. N., & Newsome, W. T. (1998). The variable discharge of cortical neurons: Implications for connectivity, computation, and information coding. *Journal of Neuroscience*, *18*, 3870–3896.

Shen, X., & De Wilde, P. (2007). Robustness and regularity of oscillations in neuronal populations. *Biosystems*, *88*, 127–136.

Song, S., Miller, K., & Abbott, L. (2000). Competitive Hebbian learning through spike-timing-dependent synaptic plasticity. *Nature Neuroscience*, *3*, 919–926.

Strogatz, S. H. (2000). From Kuramoto to Crawford: Exploring the onset of synchronization in populations of coupled oscillators. *Physica D*, *143*, 1–20.

Strogatz, S. H., Mirollo, R. E., & Matthews, P. C. (1992). Coupled nonlinear oscillators below the synchronization threshold: Relaxation by generalized Landau damping. *Physical Review Letters*, *68*, 2730–2733.

Tsodyks, M., Uziel, A., & Markram, H. (2000). Synchrony generation in recurrent networks with frequency-dependent synapses. *Journal of Neuroscience*, *20*, 1–5.

Volman, V., Baruchi, I., Persi, E., & Ben-Jacob, E. (2004). Generative modelling of regulated dynamical behavior in cultured neuronal networks. *Physica A-Statistical Mechanics and Its Applications*, *335*, 249–278.

Received August 17, 2007; accepted December 18, 2007.